

RESEARCH

Open Access



Development of a m6A- and ferroptosis-related LncRNA signature for forecasting prognosis and treatment response in cervical cancer

Kaiting Wen¹, Lili Wang¹, Huancheng Su¹, Lijun Yu^{1*}, Sanyuan Zhang^{1*}, Meiyang Wei¹, Yaling Wang¹, Le Zhao¹ and Yan Guo¹

Abstract

Background N6-methyladenosine (m6A) and ferroptosis are involved in the development and prognosis of various cancers via long noncoding RNAs (lncRNAs). This study aimed to investigate the cervical cancer subtypes based on m6A- and ferroptosis-related lncRNAs (mflncRNAs) and to construct a mflncRNA signature to predict cervical cancer prognosis and treatment response.

Methods mflncRNA-related cervical cancer subtypes were identified based on public datasets, and their differences in terms of prognosis, immune cell infiltration, and biological mechanisms were compared. Moreover, prognosis-related mflncRNAs were identified to construct a prognostic signature. A nomogram was constructed based on the independent prognostic factors. Immune characteristics, immunotherapy response predictions, and drug sensitivity analyses were performed for both risk groups. Furthermore, quantitative PCR was performed to validate the differential expression of the signature mflncRNAs in clinical samples.

Results In total, 549 differentially expressed mflncRNAs were identified between cervical cancer and normal samples. Two mflncRNA-related cervical cancer subtypes that exhibited distinct prognoses, immune characteristics, and biological mechanisms were identified. A prognostic signature was developed using six prognostic mflncRNAs: *AC016065.1*, *AC096992.2*, *AC119427.1*, *AC133644.1*, *AL121944.1*, and *FOXD1_AS1*. This prognostic signature exhibited high performance in predicting the prognosis of cervical cancer. Moreover, RiskScore and stage were identified as independent prognostic factors, and a nomogram was constructed to accurately forecast overall survival. Furthermore, patients in the low-risk group had a more active immunotherapy response and were more sensitive to chemotherapeutic drugs such as imatinib. Upregulated expression of *AC119427.1*, *AC133644.1*, *AL121944.1*, and *FOXD1_AS1* was observed in the tumor samples.

*Correspondence:

Lijun Yu
yulijun100@163.com
Sanyuan Zhang
zsyprofessor@aliyun.com

Full list of author information is available at the end of the article



© The Author(s) 2025. **Open Access** This article is licensed under a Creative Commons Attribution-NonCommercial-NoDerivatives 4.0 International License, which permits any non-commercial use, sharing, distribution and reproduction in any medium or format, as long as you give appropriate credit to the original author(s) and the source, provide a link to the Creative Commons licence, and indicate if you modified the licensed material. You do not have permission under this licence to share adapted material derived from this article or parts of it. The images or other third party material in this article are included in the article's Creative Commons licence, unless indicated otherwise in a credit line to the material. If material is not included in the article's Creative Commons licence and your intended use is not permitted by statutory regulation or exceeds the permitted use, you will need to obtain permission directly from the copyright holder. To view a copy of this licence, visit <http://creativecommons.org/licenses/by-nc-nd/4.0/>.

Conclusions The six-mfrlncRNA signature is a new biomarker for forecasting prognosis and treatment response in cervical cancer.

Keywords Cervical cancer, N6-methyladenosine, Ferroptosis, Long non-coding RNA, Prognostic signature

Introduction

Cervical cancer poses a major health challenge worldwide and is the fourth most frequently diagnosed cancer in women [1]. In 2022, cervical cancer resulted in approximately 661,021 new cases and 348,189 deaths worldwide [2]. Advancements in prevention and screening have led to a decline in the incidence and mortality rates of cervical cancer in developed countries. However, these rates remain elevated or have deteriorated in many developing countries [3]. The 5-year survival rate is 92% in patients in the early stages of the disease (IA1-IB2 and IIA1), 59% in those in the second stage of the disease (IB3, IIA2, and IIB-IVA), and 17% in those in advanced stages with distant metastases (IVB) [4]. Treatment approaches for patients with cervical cancer are tailored based on the FIGO stage and lymph node status. With precise genetic testing, targeted therapies, and immunotherapies are emerging as new models for tumor detection and treatment; however, a considerable proportion of patients show limited response to immune checkpoint inhibitors [5]. Hence, it is essential to identify promising biomarkers to improve risk stratification, prognosis, and treatment response assessment in patients with cervical cancer.

Long non-coding RNAs (lncRNAs) longer than 200 nucleotides have gained attention as potential biomarkers [6]. The lncRNAs have been implicated in the malignant development of multiple cancers and contribute to therapeutic resistance [7–9]. In cervical cancer, multiple lncRNAs play a key role in cancer diagnosis, treatment, and prognosis [10, 11]. Elevated levels of the lncRNA *HOXC-AS3* drive cervical cancer development and are indicative of a less favorable prognosis [12]. The lncRNA *ABHD11-AS1* contributes to cervical cancer progression and is key to the diagnosis and treatment of this malignancy [13]. Furthermore, lncRNA signatures are considered promising diagnostic and prognostic biomarkers for cervical cancer [14, 15].

Additionally, lncRNA regulation can be modulated by N6-methyladenosine (m6A), which affects the pathogenesis of numerous cancers [16]. m6A modifications are abundant in mammalian RNA and influence a wide range of biological processes and mRNA metabolism [17]. The m6A modification is regulated by signal transducers (readers), demethylases (erasers), and methyltransferases (writers) [18]. This modulation has profound implications in cancers, including cervical cancer, where the multifaceted role of m6A methylation offers insights into novel diagnostic, therapeutic, and prognostic approaches

[19, 20]. Furthermore, upregulation of the *FOXD2-AS1* induced by m6A methyltransferase-like 3, contributes to cervical cancer progression [21]. The prognosis of various cancers, such as cervical cancer, can be assessed using m6A-related lncRNAs [22]. Therefore, the identification of key m6A-related lncRNAs may provide new ideas for early cancer diagnosis and treatment.

Ferroptosis, a type of non-apoptotic cell death, is linked to oxidative damage [23] and is characterized by iron-dependent lipid peroxidation, resulting in plasma membrane injury [24]. Ferroptosis has a pivotal role as a regulatory mechanism of tumor proliferation that affects the efficacy of tumor treatment [25]. Ferroptosis plays a role in cervical cancer, opening new avenues for clinical research on this malignancy [26]. Ferroptosis-related genes are promising targets for developing therapeutic strategies for cancer [27]. Moreover, a potential association between m6A molecules and ferroptotic genes during cancer development has been identified [28]. *METTL14* enhances sorafenib-induced ferroptosis in cervical cancer by reducing the stability of the *FTH1* mRNA via m6A methylation [29]. However, the relationships between m6A, ferroptosis, lncRNAs, and cervical cancer remain unclear.

This study aimed to identify differentially expressed m6A- and ferroptosis-related lncRNAs (mfrlncRNAs) in cervical cancer samples using public gene expression data and analyze their differences in terms of prognosis, immune cell infiltration, and biological mechanisms. Moreover, we screened the prognosis-related mfrlncRNAs and constructed a prognostic mfrlncRNA signature. Subsequently, we established a nomogram and compared the immune characteristics, immunotherapy response, and drug sensitivity between the two risk groups. Furthermore, we validated the differential expression of the signature mfrlncRNAs in clinical samples. A workflow diagram of this study is shown in Fig. 1. The findings of this study improve our understanding of the landscape underlying cervical cancer and provide a refined framework for predicting patient outcomes and tailoring therapeutic interventions.

Materials and methods

Data acquisition and preprocessing

Data on ferroptosis-related genes were downloaded from the FerrDB v2 database [30]. After removing duplicates, 484 ferroptosis-related genes were identified. Then, 23 m6A regulators were identified, including 8 writers, 2 erasers, and 13 readers. The integrated transcriptomic

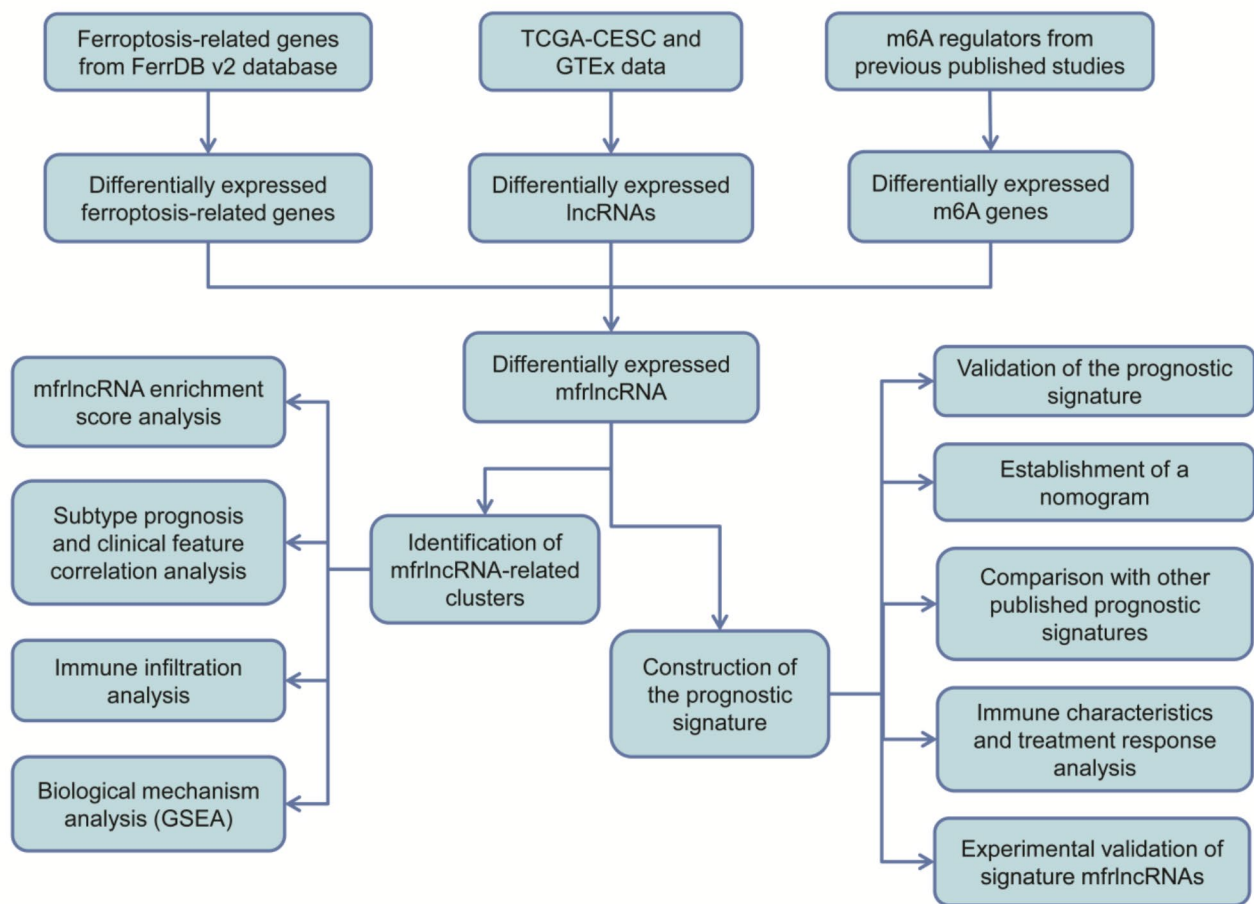


Fig. 1 The workflow diagram of this study

expression data for cervical cancer [The Cancer Genome Atlas Cervical Squamous Cell Carcinoma and Endocervical Adenocarcinoma (TCGA-CESC) and GTEx], along with the phenotypic and survival data for cervical cancer, were downloaded from the UCSC Xena database [31]. This dataset included 305 TCGA-CESC and 88 GTEx control samples.

Data preprocessing

The human reference genome *gtf* annotation file was downloaded using the `import` function in the R package `tracklayer` (version 1.64.0). The Ensembl IDs in TCGA-CESC data were converted to gene symbols, and the corresponding gene types were annotated. Genes with expression values of 0 in >80% of the samples were filtered out. The average expression value across each sample was calculated for genes that appeared multiple times. Finally, a gene expression matrix containing 31,849 genes and 393 samples and a lncRNA expression matrix containing 7,832 lncRNAs and 393 samples were obtained.

Differential expression analysis

Differentially expressed lncRNAs (DE-lncRNAs) between TCGA-CESC and GTEx control samples were identified using the R package `limma` (version 3.60.3) [32]. The threshold value for DE-lncRNAs screening was set at $p < 0.05$, and $|\log_2 \text{fold change (FC)}| > 1$. The differential expression of m6A and ferroptosis-related genes between TCGA-CESC and GTEx control samples was analyzed using the Wilcoxon rank-sum test. The differentially expressed m6A or ferroptosis-related genes were selected with a cut-off value of $p < 0.05$. Subsequently, Pearson's correlation analysis was performed to assess the correlation between DE-lncRNAs and differentially expressed m6A or ferroptosis-related genes to identify differentially expressed m6A-related lncRNAs or ferroptosis-related lncRNAs. The threshold for correlation was set at $R = 0.6$ and $p < 0.001$. The intersection of differentially expressed m6A-related lncRNAs and ferroptosis-related lncRNAs was considered an mflncRNA.

Identification of mfrlncRNA-related clusters

Based on the mfrlncRNA expression data, unsupervised clustering of TCGA-CESC tumor samples was conducted using the R package ConsensusClusterPlus (version 1.68.0) [33]. Clustering was performed using the PAM algorithm, with k ranging from 2 to 10, and Spearman correlation for distance measurement. The appropriate number of clusters (subtypes) was selected based on the heatmap and cumulative distribution plot.

Analysis of MfrlncRNA enrichment score

To evaluate the subtype results, enrichment scores of the mfrlncRNAs in each sample were calculated using the R package GSVA (version 1.50.5) [34]. The kernel function type for density estimation was set to Gaussian and the size range for the gene sets was set from 5 to 5000.

Subtype prognosis and clinical feature correlation analysis

To analyze the association between subtypes and cervical cancer prognosis, the Survfit function from the R package survival (version 3.6.4) was used to compare overall survival (OS) differences among the subtypes. Kaplan–Meier (KM) survival curves were plotted. Additionally, associations between subtypes and various clinical features were examined using the chi-square test.

Immune infiltration analysis for MfrlncRNA subtypes

To investigate the differences in tumor immune micro-environment (TIME) between subtypes, the immune infiltration levels of tumor samples in the TCGA-CESC dataset were analyzed using the CIBERSORT [35], xCell [36], and ESTIMATE [37] algorithms. The expression data of immune checkpoint-related genes were extracted from the TCGA-CESC dataset. Differences in immune infiltration scores and gene expression between the different subtypes were compared using the Wilcoxon test.

Analysis of the biological mechanism of action of MfrlncRNA subtypes

Based on the hallmark gene sets from the MSigDB database [38], the enrichment scores for each tumor sample were calculated using the R package GSVA based on the entire gene expression profile, setting the minimum and maximum gene set sizes to 5 and 5000, respectively.

To identify activated or inhibited signaling pathways, gene set enrichment analysis (GSEA) [39] was performed on the pathways. Using the classical Bayesian and linear regression methods provided by the R package, “limma,” differential expression analysis on the subtypes was performed based on gene expression data. Genes were ranked in descending order of their Log2FC values. Subsequently, the GSEA function from the R package clusterProfiler (version: 4.12.0) [40] was used to perform Kyoto Encyclopedia of Genes and Genomes (KEGG) pathway

and gene ontology (GO) enrichment analyses. The significance threshold for enrichment was set at $p < 0.05$.

Construction of the prognostic signature

By integrating the clinical data of TCGA-CESC tumor samples, the Coxph function from the R package survival [41] was utilized to conduct univariate Cox regression analysis to assess the prognostic significance of each mfrlncRNA, with a significance threshold of $p < 0.05$.

Based on the prognostic mfrlncRNAs, the sample function in R was used to divide TCGA-CESC tumor samples into training (70%) and validation (30%) datasets. A prognostic risk model was constructed based on the training dataset. First, TCGA-CESC expression data was integrated with clinical information (OS time and status). A LASSO shrinkage and selection operator regression model was built using the R package glmnet (version 4.1.8) [42]. Feature selection was performed using a 10-fold cross-validation to identify representative mfrlncRNAs. Next, based on the survival data, a Cox regression model was constructed using the R survival package. To ensure the accuracy and stability of the model, mfrlncRNAs were selected using stepwise regression. The regression coefficients (coef) [43] of the selected mfrlncRNAs were extracted from the model. By combining the regression coefficients with gene expression data, a prognostic model for cervical cancer, named the mfrlncRNA signature, was constructed as follows:

$$RiskScore = \sum_{i=1}^n (\text{gene } i) * \text{coef}$$

The optimal cut-off value for the RiskScore was determined using the surv cut-off function from the R package survminer (version: 0.4.9). Based on this optimal cut-off value, patient samples were grouped as follows: samples with a RiskScore higher than the optimal cut-off value were defined as the high-risk group, and those with a lower RiskScore were defined as the low-risk group. The KM and receiver operating characteristic (ROC) curves for 1-, 3-, and 5-year OS predictions were plotted to evaluate the predictive performance of the mfrlncRNA signature.

To validate the predictive performance of the mfrlncRNA signature, the expression data for the selected feature mfrlncRNAs were extracted from both the validation and entire datasets, and prognostic models were constructed using the same method. KM and ROC curves were used to assess the performance of the models.

Selection of independent prognostic factors

Univariate Cox regression analysis on the RiskScore, age (< 60 and ≥ 60), tumor-node-metastasis (TNM) stage, American Joint Committee on Cancer stage, and tumor

grade was performed. Features with $p < 0.05$ were considered to be related to prognosis. Next, a multivariate Cox regression analysis of these features was performed, and features with $p < 0.05$ were considered independent prognostic factors.

Establishment of a nomogram

To facilitate the prediction of OS probability of patients with cervical cancer, a nomogram was established based on independent prognostic factors using the R package rms (version 6.8.1). To validate the nomogram, calibration curves, decision curve analysis (DCA) plots, and ROC curves were generated to assess performance.

Comparison with other published prognostic signatures

To validate the performance of the mfrlncRNA signature, published prognostic signatures from previous studies on cervical cancer were retrieved. Using our model, the concordance index (C-index) for each prognostic signature was calculated and compared with the C-index of our mfrlncRNA signature in TCGA training, validation, and the entire datasets.

Analysis of immune characteristics and treatment responses related to the MfrlncRNA signature

To evaluate the role of the mfrlncRNA signature in the TIME of cervical cancer, the relationship among the mfrlncRNA signature, immune cell infiltration, and immune regulators was investigated. TIME was assessed using the CIBERSORT [44], TIMER [45], EPIC [46], xCell [36], and MCPcounter [47] algorithms with the R package IOBR (version: 0.99.8) [48]. Subsequently, the association between the mfrlncRNA signature and most immune regulators, including ligands and receptors, was examined. The immunotherapy response and drug sensitivity associated with the mfrlncRNA signature were analyzed. Based on gene expression data, the immunotherapy response of the samples was assessed using the tumor immune dysfunction and exclusion (TIDE) database. The microsatellite instability (MSI), immune profile score (IPS), interferon gamma (IFNG), and TIDE scores of the two risk groups were compared using the Wilcoxon test, with the significance threshold set at $p < 0.05$. Furthermore, the Cancer Drug Sensitivity Genomics Database (GDSC, <https://www.cancerrxgene.org/>) [49] was used to estimate each patient's sensitivity to chemotherapeutic drugs. The IC50 of each drug was quantified using the R package, pRRophetic (version 0.5), and the differences between the two risk groups were analyzed using the Wilcoxon rank-sum test. Additionally, as many proteins lacked binding sites or had insufficient affinity for small molecules and antibodies, potential drug targets were collected from previous studies and Spearman's

rank correlation analysis was used to screen targets associated with the RiskScore.

Experimental validation

From June 2023 to January 2024, 10 pairs of tumor and adjacent non-cancerous tissue samples were collected from patients with cervical cancer who underwent primary surgical resection at the First Hospital of Shanxi Medical University. Our study was approved by the Ethics Committee of the First Hospital of Shanxi Medical University (NO.KYYJ-2023-161). All patients provided informed consent for this study.

Quantitative polymerase chain reaction (qPCR) was used to validate the expression of mfrlncRNAs in the prognostic signatures. In brief, total RNA was extracted from clinical tissue samples using RNAiso Plus (Trizol) reagent (TaKaRa, Japan). After reverse transcription to cDNA using the ReverTra Ace[®] qPCR RT master mix (TOYOBO, Japan), real-time qPCR was performed using Power SYBR Green PCR master mix (Thermo, USA). The relative lncRNA expression was quantified using the $2^{-\Delta\Delta C_t}$ method using GAPDH as the internal control.

Statistical analysis

The experimental data are expressed as mean standard deviation (SD). Statistical analyses were performed using GraphPad 9.0.5 software (GraphPad Software, San Diego, CA, USA). The differences between groups were analyzed using one-way analysis of variance (ANOVA), with $p < 0.05$ indicating statistical significance.

Results

Identification of MfrlncRNAs

Using differential expression analysis, 3,100 DE-lncRNAs (1,370 upregulated and 1,730 downregulated) were identified between TCGA-CESC and GTEx control samples (Fig. 2a). Additionally, 23 differentially expressed m6A genes (Fig. 2b) and 417 ferroptosis-related genes (Fig. 2c) were identified. Pearson correlation analysis identified 551 differentially expressed m6A-related lncRNAs and 1,656 differentially expressed ferroptosis-related lncRNAs. In total, 549 mfrlncRNAs were identified in intersectional analysis (Fig. 2d).

Identification of MfrlncRNA subtypes

Before clustering, the sample numbers of TCGA-CESC were matched with the sample numbers in the survival data, and samples with a survival time of 0 were excluded, leaving a total of 292 CESC samples. Based on the expression data of 549 mfrlncRNAs, unsupervised clustering analysis showed that when the optimal number of clusters (k) = 2, the heatmap divisions were clearer than the other values (Fig. 3a) and the cumulative distribution function was closest to being parallel to the x-axis

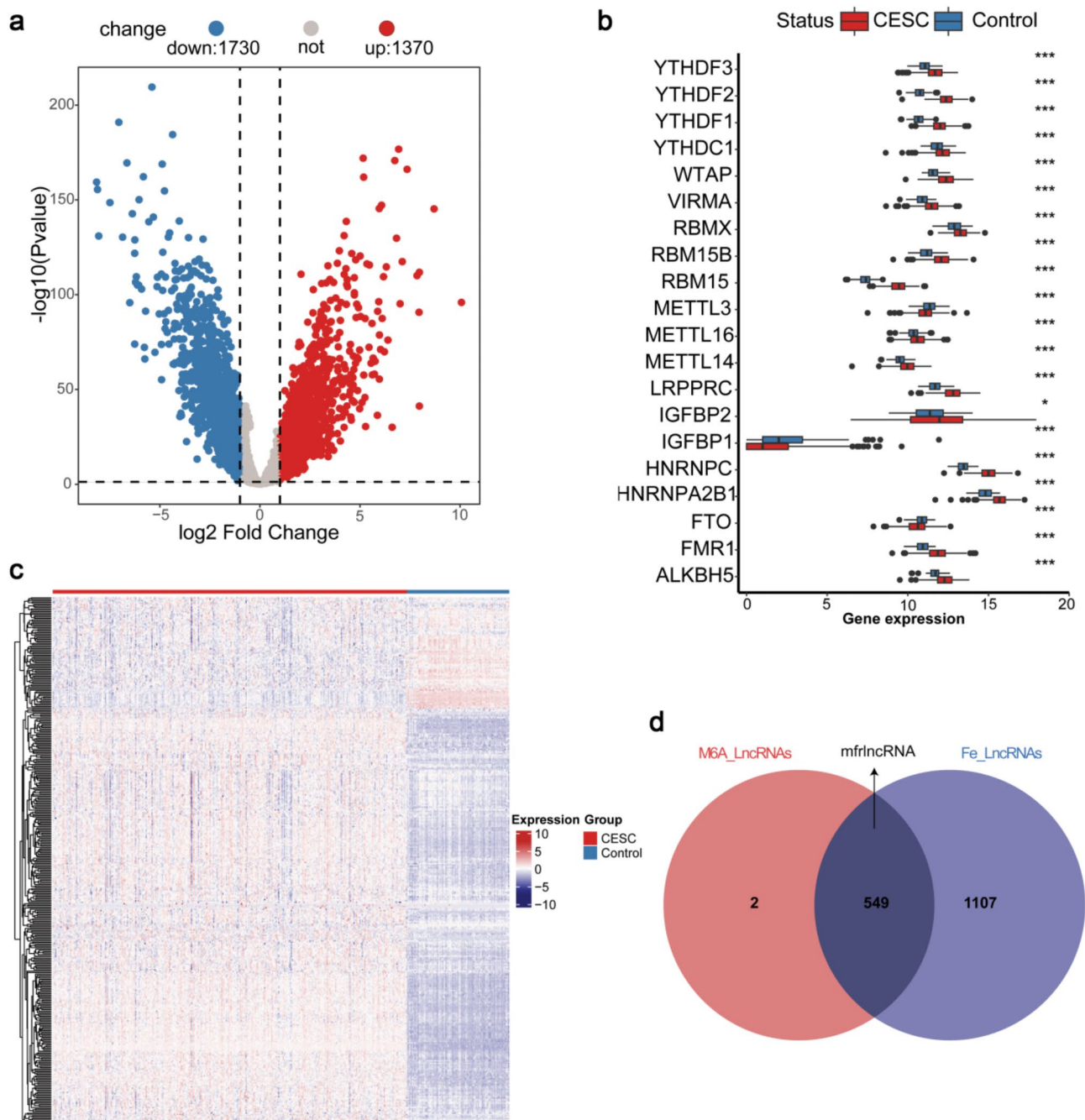


Fig. 2 Identification of mfrlncRNAs. **(a)** Volcano plot of differentially expressed lncRNAs between TCGA-cervical cancer ($n = 305$) and GTEx control ($n = 88$) samples. Red nodes indicate upregulated lncRNAs and blue nodes indicate downregulated lncRNAs. **(b)** Box plots of 23 differentially expressed m6A genes. * $p < 0.05$ and *** $p < 0.001$. **(c)** Expression heatmap of 417 differentially expressed ferroptosis genes. **(d)** Venn diagram of differentially expressed m6A-related and ferroptosis-related lncRNAs. mfrlncRNAs: m6A- and ferroptosis-related lncRNAs

(Fig. 3b). Therefore, k was 2, which divided the tumor samples into two subtypes. Clusters 1 and 2 included 122 and 170 samples, respectively. Subsequently, we used GSVA to calculate the mfrlncRNA score of the cervical cancer samples in the two clusters and found that cluster 1 had a notably higher mfrlncRNA score than cluster 2 ($p = 5.5e-15$; Fig. 3c), indicating a significant difference

between the two subtypes. Moreover, principal component analysis showed a clear clustering of samples within the same cluster (Fig. 3d). KM curve analysis showed that patients in cluster 2 had a shorter OS time than those in cluster 1 ($p = 0.025$, Fig. 3e), indicating that cluster 2 had worse prognosis. The correlation between the two subtypes and various clinical factors such as age, TNM stage,

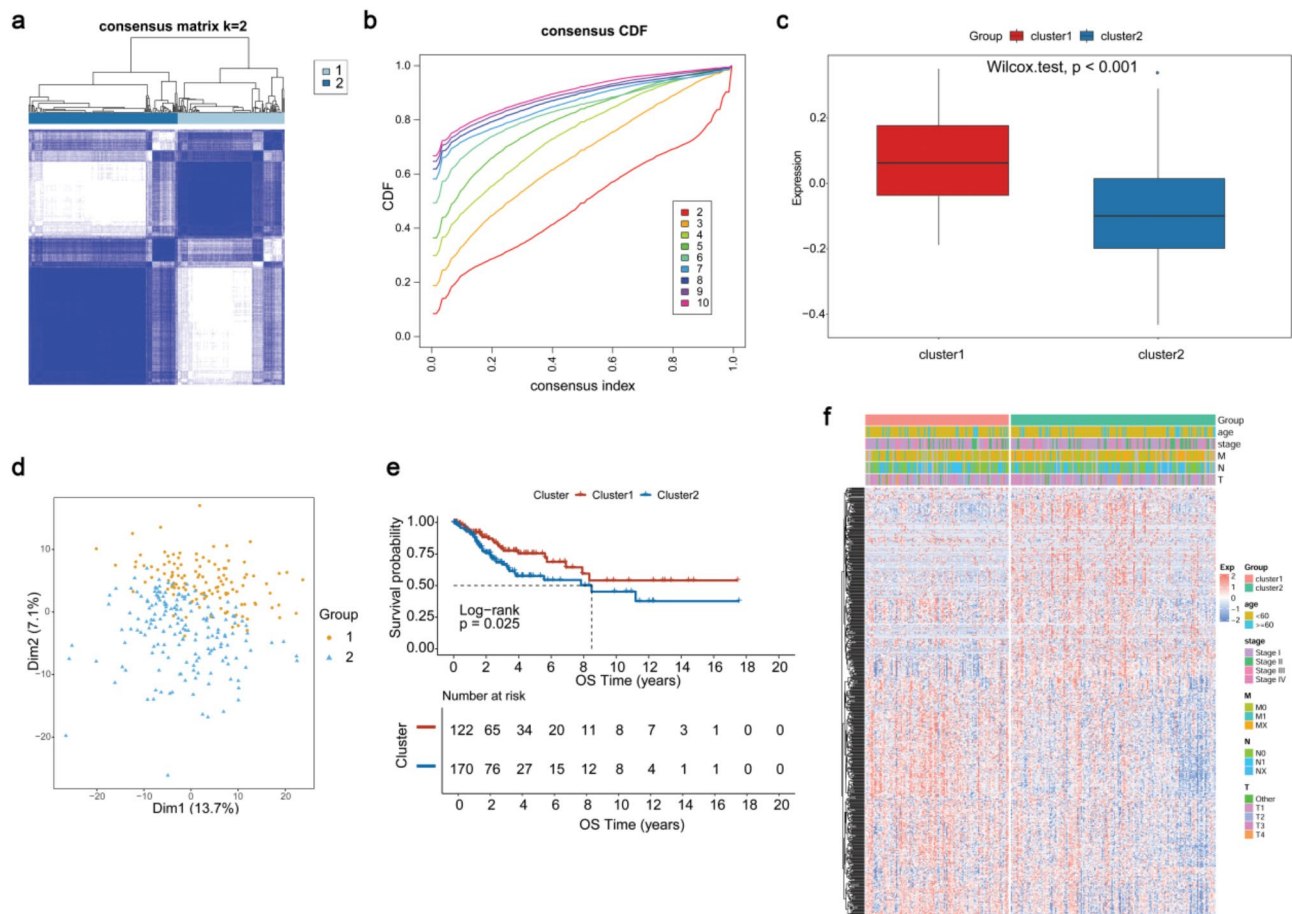


Fig. 3 Identification of mflncRNAs subtypes. **(a)** Heatmap of sample distribution with different cluster numbers (clusters 1, 122 samples; cluster 2, 170 samples). **(b)** CDF distribution curve. **(c)** Comparison of the mflncRNA score of two clusters. **(d)** PCA plot of sample distribution in the two clusters. **(e)** Kaplan–Meier survival curve of the two clusters. **(f)** Heatmap showing the correlation between two subtypes and various clinical factors such as age, TNM stage, and overall stage. mflncRNAs: m6A-and ferroptosis-related lncRNAs; CDF: cumulative distribution function; PCA: principal component analysis

and overall stage is shown in Fig. 3f. The distribution of various clinical factors in two subtypes was displayed and there was no close association between the subtypes and age, tumor stage, and TNM classification.

Comparison of immune characteristics and biological mechanisms between the two subtypes

Based on TCGA-CESC data, the proportion of infiltrating immune cells was analyzed. The xCell algorithm identified multiple cell types that were significantly associated with subtypes, including T regulatory cells, MSCs, MEPs, and CD8+ Tem cells (Fig. 4a). Using the CIBERSORT algorithm, five types of immune cells were significantly related to the following subtypes: CD4+ memory resting T cells, memory B cells, naïve B cells, eosinophils, and follicular helper T cells (Fig. 4b). Dramatically higher ESTIMATE and stromal scores were observed in cluster 2 than in cluster 1 (Fig. 4c). Furthermore, immune checkpoint genes, including *BTLA*, *TNFRSF4*, and *TNFRSF9*, showed higher expression levels in cluster 2 (Fig. 4d).

These data indicated that the two subtypes exhibited distinct immune characteristics.

Next, we analyzed the differences in the 50 pathways between the two subtypes based on the GSVA enrichment scores. Among these, 28 pathways, including HALLMARK_REACTIVE_OXYGEN_SPECIES_PATHWAY, HALLMARK_OXIDATIVE_PHOSPHORYLATION, and HALLMARK_DNA_REPAIR, differed significantly among the subtypes (Fig. 4e). Moreover, GSEA was conducted to identify differential GO functions and KEGG pathways between the two subtypes. As a result, 3,294 differential GO functions, such as the immune response-regulating cell surface receptor signaling pathway (Fig. 4f), and 145 differential pathways, such as ribosomes (Fig. 4g), were enriched.

Construction and validation of the MflncRNA signature

By integrating clinical data from TCGA-CESC samples, 103 mflncRNAs were found to be related to OS. Subsequently, LASSO Cox analysis identified 11

(See figure on previous page.)

Fig. 4 Comparison of the immune characteristics and biological mechanisms of action of the two subtypes (clusters 1, $n=122$; cluster 2, $n=170$). **(a)** Comparison of the results regarding immune cell infiltration obtained using the xCell algorithm between the two clusters. **(b)** Comparison of the results regarding immune cell infiltration obtained using the CIBERSORT algorithm between the two clusters. **(c)** Comparison of the results regarding ESTIMATE score, immune score, and stromal score obtained using the ESTIMATE algorithm between the two clusters. **(d)** Comparison of the expression of immune checkpoint genes between the two clusters. **(e)** Results of GSVA pathways in the two clusters. **(f)** GSEA analysis showed the differential GO functions between the two clusters. **(g)** GSEA analysis showed the differential KEGG pathways between the two clusters. * $p < 0.05$, ** $p < 0.01$, *** $p < 0.001$, and **** $p < 0.0001$

risk-associated mfrlncRNAs (Fig. 5a): *AC008438.1*, *AC008894.2*, *AC016065.1*, *AC090617.3*, *AC096992.2*, *AC119427.1*, *AC131953.1*, *AC133644.1*, *AL121944.1*, *AL158825.2*, and *FOXD1_ASI*. To ensure the accuracy and stability of the model, stepwise multivariate regression was conducted to screen the mfrlncRNAs for prognostic model construction. The optimal model included six mfrlncRNAs: *AC016065.1*, *AC096992.2*, *AC119427.1*, *AC133644.1*, *AL121944.1*, and *FOXD1_ASI* (Fig. 5b). The regression coefficients (coefs) of these mfrlncRNAs were extracted to construct a prognostic signature. The RiskScore was then calculated as follows: RiskScore = $AC016065.1 \times (-0.45035) + AC096992.2 \times (-0.49051) + AC119427.1 \times 0.467227 + AC133644.1 \times (-0.36185) + AL121944.1 \times (-0.4462) + FOXD1_ASI \times (-0.11495)$. Risk grouping for samples in the training dataset was then performed using the optimal cut-off value for the RiskScore. The high-risk and low-risk groups contained 71 and 221 patients, respectively. KM curve analysis revealed a markedly shorter OS time in the high-risk group. Moreover, patients in the high-risk group were more likely to die, and ROC curve analysis demonstrated that the area under the curve values for forecasting 1-, 3-, and 5-year OS were 0.891, 0.773, and 0.797, respectively (Fig. 5c). Consistent results were obtained based on the validation (Fig. 5d) and entire datasets (Fig. 5e), revealing the robustness of the mfrlncRNA signature. Besides, we analyzed the predictive performance of TNM stage in forecasting OS based on the entire dataset. We found that the area under the curve values for the T, N, M stages in predicting 1-, 3-, and 5-year OS were ranged from 0.548 to 0.747, all of which were lower than that of the risk score (Fig. 5f). These data demonstrated that our constructed mfrlncRNA signature had a higher predictive performance than TNM stage.

Construction of a nomogram

After constructing the prognostic signature, we compared the risk scores across different clinical feature groups, including age, tumor grade, stage, TNM, and subtypes. We observed significant differences between stages I and IV, T2 and T3, G2 and G3, and G3 and Gx, as well as between the two subtypes (Fig. 6a), indicating that the mfrlncRNA signature has good potential for clinical applications. We then investigated independent prognostic factors for cervical cancer. Stage ($p=0.002$) and risk score ($p=0$) were significant in both univariate

and multivariate regression analyses (Fig. 6b-c), indicating that these two features are independent prognostic factors. Additionally, the hazard ratios were > 1 , suggesting that these were risk factors. Using these independent prognostic factors, a nomogram was established to predict OS (Fig. 6d). The DCA curves indicated that the 1-year nomogram model was the most consistent, whereas the other nomogram models were largely consistent with the ideal model (Fig. 6e), revealing a satisfactory overlap in the predictive and actual 1-, 3-, and 5-year OS (Fig. 6f). Furthermore, to determine whether the mfrlncRNA signature has superior predictive ability, we retrieved published prognostic signatures from previous studies on cervical cancer and calculated the C-index using our model. Based on the training set, we observed that our mfrlncRNA signature had the highest C-index, suggesting the high performance of our model. However, in the comparison of the C-indices for the validation set and the entire dataset, our model ranked 10th (Fig. 6g). Although the C-indices for the validation set and the entire dataset were not the highest, the C-index of our model for the validation set and the entire dataset was higher than 0.6, suggesting a good performance.

Immune characteristics related to the MfrlncRNA signature

We evaluated the role of the mfrlncRNA signature in the TIME in cervical cancer. As shown in Fig. 7a, the mfrlncRNA signature correlated weakly with the infiltration of multiple immune cells. Moreover, the mfrlncRNA signature was related to various immune regulators, especially HLA molecules (Fig. 7b). Moreover, we investigated the performance of the mfrlncRNA signature in predicting immunotherapy responses. We found that MSI, IPS, and IFNG levels were dramatically higher in the low-risk group than in the high-risk group ($p < 0.05$; Fig. 7c), suggesting that low-risk patients had a more active immunotherapy response. However, TIDE scores did not differ significantly between the two groups. Furthermore, we estimated the sensitivity of patients to 138 chemotherapeutic drugs based on the expression data of cervical cancer samples obtained from TCGA. We observed that the IC50 values of 17 chemotherapeutic drugs differed significantly between the two risk groups. The top three drugs were imatinib, AZD.0530, and NSC.87,877, all of which exhibited higher IC50 values in low-risk patients, implying that these patients had greater drug sensitivity (Fig. 7d). Additionally, we collected potential drug targets

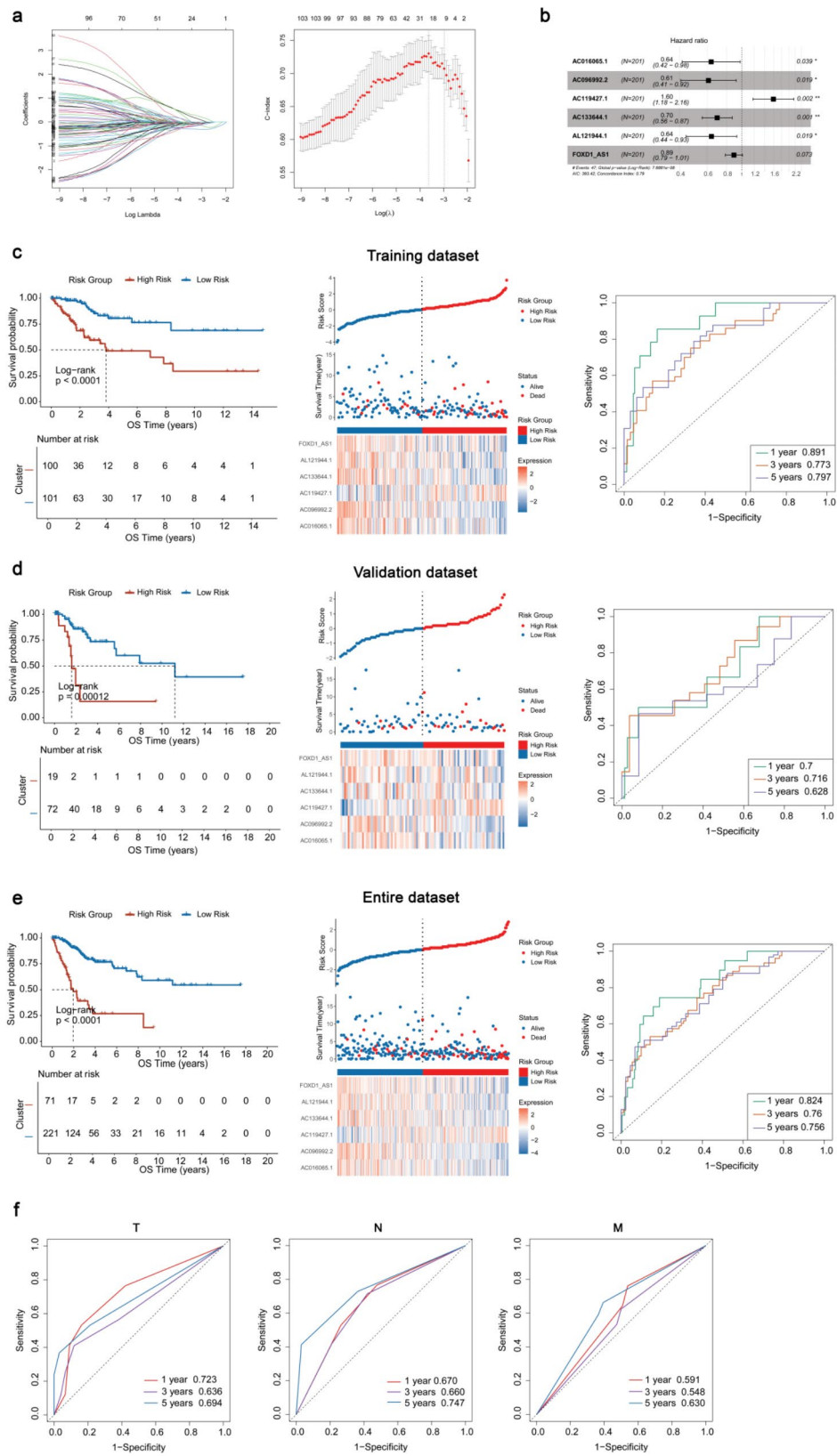


Fig. 5 (See legend on next page.)

(See figure on previous page.)

Fig. 5 Construction and validation of the mflncRNA signature. **(a)** LASSO coefficient spectrum of the prognostic mflncRNAs and optimized lambda determined in the LASSO regression model. **(b)** Forest plot of the mflncRNAs selected by the stepwise regression model in the training dataset. **(c)** Validation of the predictive performance of the prognostic signature based on the training dataset. **(d)** Validation of the predictive performance of the prognostic signature based on the validation dataset. **(e)** Validation of the predictive performance of the prognostic signature based on the entire dataset. **(f)** Analysis of the predictive performance of T, N, M stages based on the entire dataset

from previous studies, and subsequent correlation analysis revealed that 18 drug targets, including CYP2J2, were significantly associated with high-risk cervical cancer ($r > 0.2$, $p < 0.05$).

Validation of MflncRNA expression in clinical samples

To preliminarily reveal the role of key mflncRNAs in cervical cancer, qPCR was performed to validate the expression of the six signature mflncRNAs in clinical samples. The results showed that the expression of *AC119427.1*, *AC133644.1*, *AL121944.1*, and *FOXD1_ASI* in tumor tissues was higher than that in normal tissues ($p < 0.05$, Fig. 8), which is consistent with the results of the above public data analysis. However, the expression of *AC016065.1* and *AC096992.2* did not differ significantly between tumor and normal samples.

Discussion

Cervical cancer is a cause of health concern that significantly affects life expectancy and results in substantial treatment costs. Although treatments such as radiation, surgery, immunotherapy, and chemotherapy are promising, drug resistance, recurrence, and metastasis pose significant barriers to clinical management and patient survival [50]. Therefore, identification of promising biomarkers, development of reliable prognostic models, and refinement of therapeutic approaches are imperative. In this study, we identified 549 differentially expressed mflncRNAs between cervical cancer and normal samples and two mflncRNA-related cervical cancer subtypes. Two subtypes exhibited distinct prognoses, immune characteristics, and biological mechanisms. An mflncRNA signature was constructed. This signature allowed for the stratification of patients into risk groups that differed in terms of prognosis and treatment response.

Cervical cancer is a heterogeneous disease, resulting in diverse phenotypes and varying clinical outcomes. Given the variation in phenotypes and prognoses among cancer patients, personalized treatment plans can enhance patient outcomes, emphasizing the importance of tumor subtype identification in clinical practice. With advancements in sequencing technologies and related methodologies, molecular subtyping of cervical cancer based on genetic factors has gained widespread attention, offering more comprehensive insights regarding tumor biology than traditional classification systems. lncRNAs have emerged as crucial non-coding gene markers and are increasingly being recognized for their involvement in the initiation, progression,

and metastasis of various cancers, including cervical cancer [51, 52]. Ferroptosis has been implicated in numerous diseases, including cervical cancer [53]. Among the various RNA modifications, m6A regulators have shown potential as prognostic biomarkers, with their expression, mutation status, and RNA modification features being closely linked to patient survival [54]. We identified 23 differentially expressed m6A genes and 417 differentially expressed ferroptosis-related genes. Correlation and intersection analyses identified 549 differentially expressed mflncRNAs. Based on mflncRNA expression, consensus cluster analysis categorized the cervical cancer samples into two clusters, with cluster 2 displaying a worse prognosis than cluster 1. These findings offer important insights regarding cervical cancer heterogeneity and its potential prognostic implications. Additionally, cluster 2 exhibited significantly higher ESTIMATE and stromal scores, as well as higher expression of immune checkpoint-related genes such as *BTLA*, *TNFRSF4*, and *TNFRSF9*. These results suggest that cluster 2 may have a stronger immune response, potentially influencing prognosis and immunotherapy response. Furthermore, we performed GESA to elucidate the differentially enriched pathways, including ribosomes, between the two subtypes. Ribosomes are critical for the synthesis of functional proteins, and ribosome biogenesis is crucial for cancer metastasis and treatment resistance [55]. Therefore, we speculated that key pathways, such as ribosome biogenesis, may be responsible for the varying prognoses of patients with different mflncRNA subtypes.

Previous studies have developed prognostic signatures to predict outcomes in patients with cervical cancer based on lncRNAs, ferroptosis, m6A regulators, or combinations of these biomarkers [56–58]; however, an accurate and clinically applicable prognostic signature specifically focusing on mflncRNAs for patients with cervical cancer remains to be established. To better predict patient prognosis and treatment response, we constructed a prognostic signature based on six prognostic mflncRNAs: *AC016065.1*, *AC096992.2*, *AC119427.1*, *AC133644.1*, *AL121944.1*, and *FOXD1_ASI*. *FOXD1_ASI* promotes the development of numerous cancers [59–61]. However, the role of other five mflncRNAs in cancer remains largely unknown. Nevertheless, our study confirmed the upregulation of *AC119427.1*, *AC133644.1*, *AL121944.1*, and *FOXD1_ASI* in clinical cervical cancer tissues, indicating that these mflncRNAs may be involved in the development of cervical cancer. The potential role of these mflncRNAs as key contributors to cervical cancer development warrants further investigation. Furthermore,

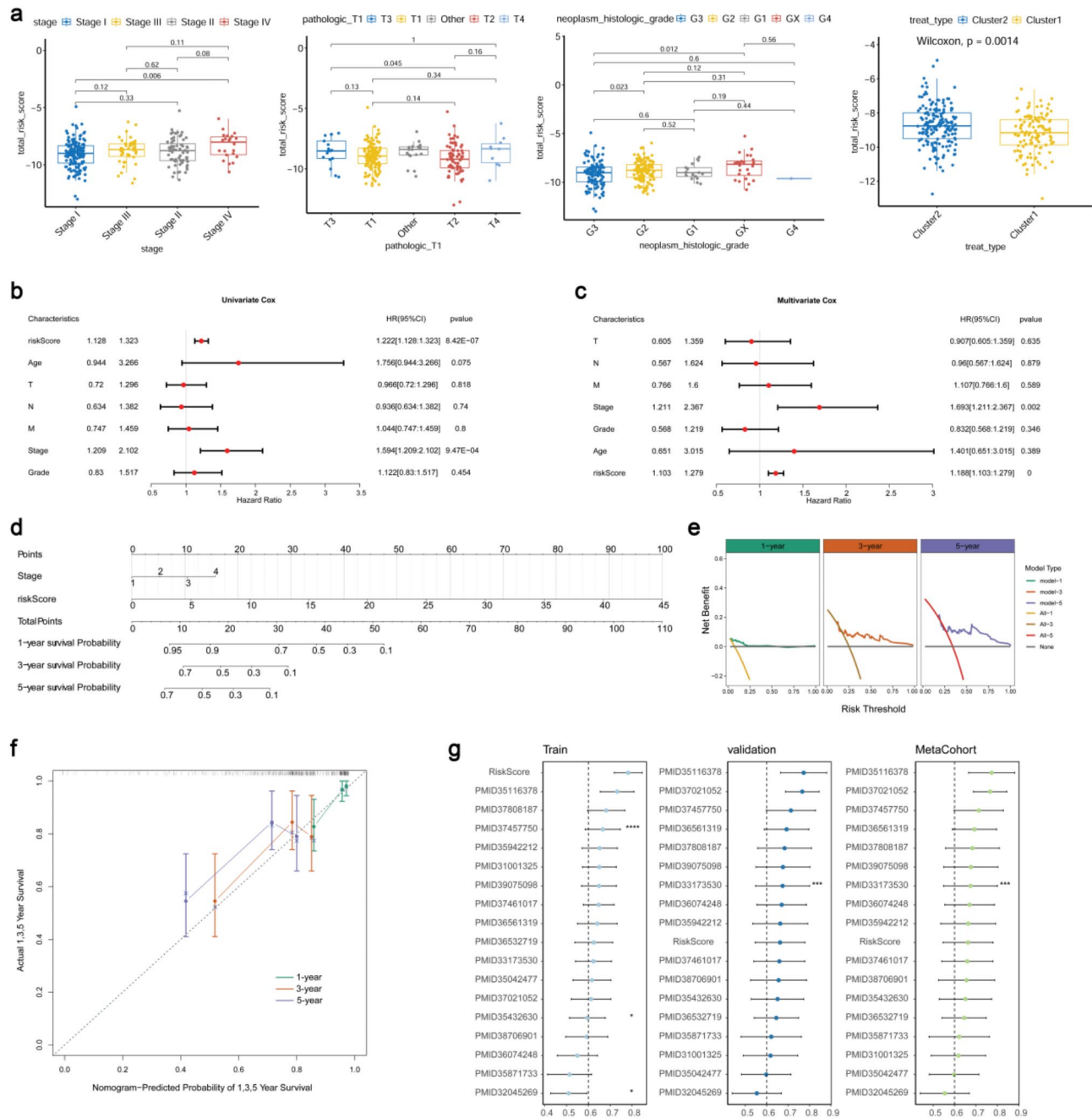


Fig. 6 Prognostic value of RiskScore and construction of a nomogram. **(a)** Comparison of the risk scores across different clinical feature groups, including age, tumor grade, stage, TNM, and subtypes. **(b)** Univariate Cox regression analysis for screening prognostic factors. **(c)** Multivariate Cox regression analysis for screening independent prognostic factors. **(d)** The constructed nomogram. **(e)** DCA curves for assessing nomogram performance. **(f)** Calibration curves for assessing nomogram performance. **(g)** Comparing the performance of the mfrlncRNA signature with various published prognostic signatures based on training, validation, and entire datasets

our established mfrlncRNA signature demonstrated a strong predictive power for cervical cancer prognosis. Therefore, we propose that this mfrlncRNA signature could be a valuable prognostic tool, with these mfrlncRNAs acting as promising biomarkers for cervical cancer prognosis.

TIME is composed of various types of immune cells, and tumor-infiltrating immune cells are closely associated with

cancer development and have a significant impact on the therapeutic and prognostic outcomes of antitumor interventions [62, 63]. This study evaluated the role of the mfrlncRNA signature in the TIME of cervical cancer and revealed that the signature correlated with multiple immune cell infiltrations and various immune regulators, especially HLA molecules, which are related to cervical cancer susceptibility

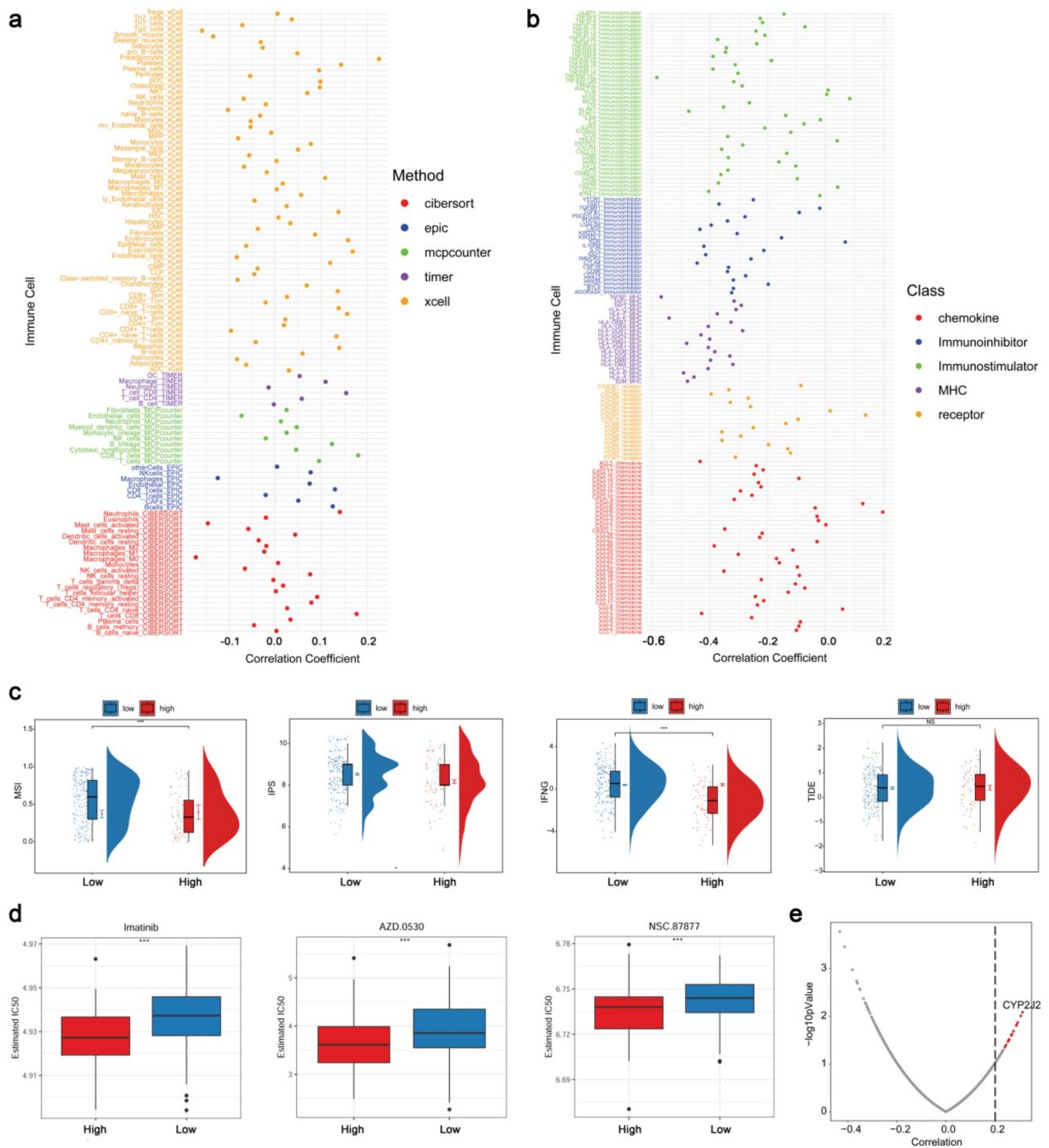


Fig. 7 Immune characteristics related to the mflncRNA signature and analysis of treatment response of the two risk groups (high risk group, $n=71$; low risk group, $n=221$). **(a)** Correlation between the mflncRNA signature and multiple immune cell infiltrations. **(b)** Correlation between the mflncRNA signature and various immune regulators. **(c)** Comparison of immunotherapy response indicators between the two risk groups. **(d)** The top three chemotherapeutic drugs, the sensitivities of which differed significantly between the risk groups. **(e)** Analysis of potential drug targets related to high-risk score. * $p < 0.05$, ** $p < 0.01$, and *** $p < 0.001$ compared to normal tissues

[64]. HLA genes are vital regulators of immune recognition and presentation, and their expression is closely linked to immunological features of tumors and patient prognosis [65]. Additionally, we found that the MSI, IPS, and IFNG

levels were dramatically higher in the low-risk group, indicating that low-risk patients had a more active immunotherapy response. Finally, drug sensitivity analysis demonstrated that low-risk patients exhibited greater sensitivity to several

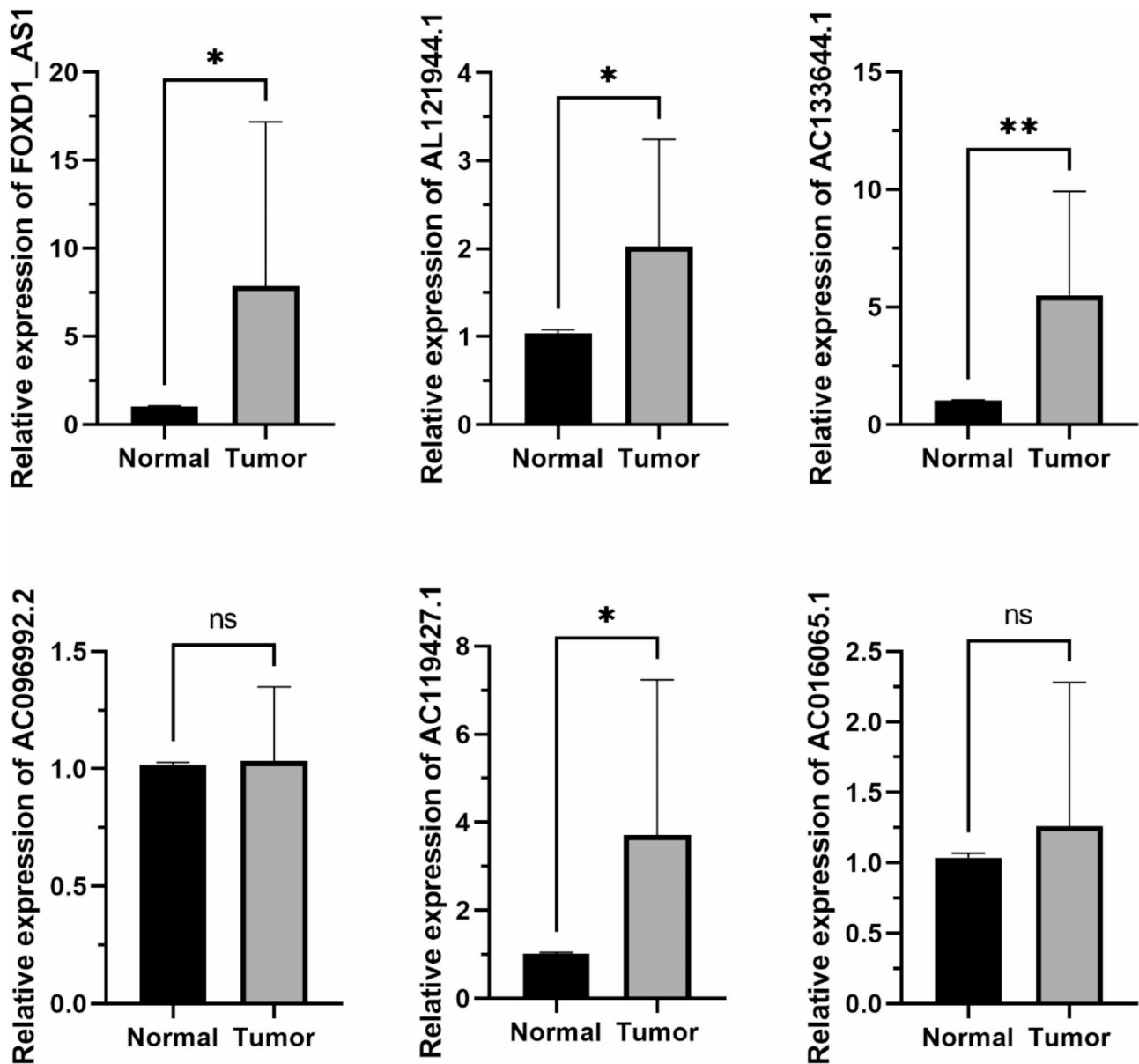


Fig. 8 Validation of the expression of signature mflncRNAs in clinical samples ($n = 10$ each group). * $p < 0.05$ and ** $p < 0.01$ compared to normal tissues

drugs, such as imatinib. Overall, these data provide new insights that will be useful for drug screening and making treatment decisions for patients with cervical cancer.

This is the first study to characterize mflncRNA-related cervical cancer subtypes and develop a prognostic mflncRNA signature. This signature enables the stratification of patients into distinct risk groups, offering potential benefits in terms of predicting prognosis and developing tailored treatment approaches for patients with different risks. However, this study has several limitations. First, the clinical sample size for validation was small, which may reduce the statistical power of the findings. Second, we did not validate the prognostic value of the mflncRNA signature in a clinical cohort. Additionally, because the mflncRNA signature

is related to prognosis and treatment response in cervical cancer, incorporating its detection in blood serum—an approach that is non-invasive, cost-effective, and feasible—could further enhance the clinical relevance of this study. More clinical trials are needed to confirm the practicality and accuracy of this model for predicting immunotherapy outcomes in patients with cervical cancer. Lastly, the regulatory mechanisms underlying these mflncRNAs in cervical cancer are yet to be investigated. In summary, further prospective studies and foundational research are essential to improve our understanding and refine the findings of this study.

In conclusion, this study identified a panel of lncRNAs linked to both m6A regulators and ferroptosis-related genes

and established a mflncRNA signature for patient stratification. The mflncRNA signature demonstrated significant prognostic potential and could predict the treatment response in patients with cervical cancer. These findings shed light on the molecular mechanisms that drive cervical cancer progression and offer a promising tool for developing personalized medicine, paving the way for more accurate prognostic assessments and innovative therapeutic approaches in clinical practice.

Abbreviations

m6A	N6-methyladenosine
lncRNAs	Long noncoding RNAs
mflncRNAs	m6A-and ferroptosis-related lncRNAs
TCGA-CESC	The Cancer Genome Atlas - Cervical Squamous Cell Carcinoma and Endocervical Adenocarcinoma
DE-lncRNAs	Differentially expressed lncRNAs
FC	Fold change
KM	Kaplan–Meier
TIME	Tumor immune microenvironment
GSEA	Gene set enrichment analysis
KEGG	Kyoto Encyclopedia of Genes and Genomes
GO	Gene ontology
ROC	Receiver operating characteristic
TNM	Tumor-node-metastasis
DCA	Decision curve analysis
C-index	Concordance index
TIDE	Tumor immune dysfunction and exclusion
MSI	Microsatellite instability
IPS	Immune profile score
IFNG	Interferon gamma
GDSC	Cancer Drug Sensitivity Genomics Database
qPCR	Quantitative polymerase chain reaction
SD	Standard deviation
ANOVA	Analysis of variance

Acknowledgements

We would like to express our gratitude for the technical support offered by TCGA and GTEx in sharing the data, as well as to the authors for their valuable contributions to this study.

Author contributions

KW, LY, and SZ contributed to the study conception and design of the study. Material preparation, data collection, and analysis were performed by KW, LW, HS, and MW collected the samples. YW, LZ, and YG performed the experiments. KW wrote the first draft of the manuscript and all authors commented on earlier versions of the manuscript. All authors read and approved the final version of the manuscript.

Funding

The research that led to these results received no specific funding.

Data availability

The datasets used and/or analysed during the current study are available from the corresponding author on reasonable request.

Declarations

Ethics approval and consent to participate

Our study was approved by the Ethics Committee of the First Hospital of Shanxi Medical University (NO.KYYJ-2023-161). All patients provided informed consent for the study.

Consent for publication

Not applicable.

Competing interests

The authors declare no competing interests.

Author details

¹Department of Gynecology, First Hospital of Shanxi Medical University, No. 85 Jiefang South Road, Taiyuan, Shanxi 030001, China

Received: 3 December 2024 / Accepted: 19 March 2025

Published online: 31 March 2025

References

- Yadav G, Srinivasan G, Jain A. Cervical cancer: novel treatment strategies offer renewed optimism. *Pathol Res Pract*. 2024;254:155136.
- Bray F, Laversanne M, Sung H, Ferlay J, Siegel RL, Soerjomataram I, Jemal A. Global cancer statistics 2022: GLOBOCAN estimates of incidence and mortality worldwide for 36 cancers in 185 countries. *Cancer J Clin*. 2024;74(3):229–63.
- Cohen PA, Jhingran A, Oaknin A, Denny L. Cervical cancer. *Lancet (London England)*. 2019;393(10167):169–82.
- Siegel RL, Miller KD, Wagle NS, Jemal A. Cancer statistics, 2023. *CA Cancer J Clin*. 2023;73(1):17–48.
- Mao Z, Wang B, Zhang T, Cui B. The roles of m6A methylation in cervical cancer: functions, molecular mechanisms, and clinical applications. *Cell Death Dis*. 2023;14(11):734.
- Iaccarino I, Klapper W. lncRNA as cancer biomarkers. *Methods Mol Biology (Clifton NJ)*. 2021;2348:27–41.
- Li J, Hou F, Teng Z, Xia W, Peng J. lncRNA HOXC-AS3 accelerates malignant proliferation of cervical cancer cells via stabilizing KDM5B. *J Cancer Res Clin Oncol*. 2024;150(6):294.
- An L, Dong K, Chi S, Wei S, Zhang J, Yu Z, Zhang Q, Zhang T, Cheng S, Shi R, et al. lncRNA UCA1 promotes tumor progression by targeting SMARCD3 in cervical cancer. *Mol Carcinog*. 2024;63(3):384–99.
- Aswathy R, Sumathi S. Defining new biomarkers for overcoming therapeutical resistance in cervical cancer using lncRNA. *Mol Biol Rep*. 2023;50(12):10445–60.
- Shi D, Zhang C, Liu X. Long noncoding RNAs in cervical cancer. *J Cancer Res Ther*. 2018;14(4):745–53.
- Aalijahan H, Ghorbian S. Long non-coding RNAs and cervical cancer. *Exp Mol Pathol*. 2019;106:7–16.
- Zhao R, Song J, Jin Y, Liu Y. Long noncoding RNA HOXC-AS3 enhances the progression of cervical cancer via activating erbb signaling pathway. *J Mol Histol*. 2021;52(5):991–1006.
- Zhu D, Hao Q, Qian M, Hu Y, Wu F. lncRNA ABHD11-AS1 participates in the progression of cervical carcinoma by targeting miR-1254 and is the key to the diagnosis and treatment of cervical carcinoma in the future. *J Healthcare Eng*. 2022;2022:8387458.
- Luo W, Wang M, Liu J, Cui X, Wang H. Identification of a six lncRNAs signature as novel diagnostic biomarkers for cervical cancer. *J Cell Physiol*. 2020;235(2):993–1000.
- Ping Q, Chen Q, Li N. Identification of m(6)A-related lncRNAs prognostic signature for predicting immunotherapy response in cervical cancer. *SLAS Technol*. 2024;29(6):100210.
- Chen Y, Lin Y, Shu Y, He J, Gao W. Interaction between N(6)-methyladenosine (m(6)A) modification and noncoding RNAs in cancer. *Mol Cancer*. 2020;19(1):94.
- Li J, Yang F, Wang Z, Zheng S, Zhang S, Wang C, He B, Wang JB, Wang H. METTL16-mediated N6-methyladenosine modification of Soga1 enables proper chromosome segregation and chromosomal stability in colorectal cancer. *Cell Prolif*. 2024;57(5):e13590.
- Zaccara S, Ries RJ, Jaffrey SR. Reading, writing and erasing mRNA methylation. *Nat Rev Mol Cell Biol*. 2019;20(10):608–24.
- Tang J, Zhang J, Lu Y, He J, Wang H, Liu B, Tu C, Li Z. Novel insights into the multifaceted roles of m(6)A-modified lncRNAs in cancers: biological functions and therapeutic applications. *Biomark Res*. 2023;11(1):42.
- Gao Y, Guo Q, Yu L. m6A modification of RNA in cervical cancer: role and clinical perspectives. *RNA Biol*. 2024;21(1):49–61.
- Ji F, Lu Y, Chen S, Lin X, Yu Y, Zhu Y, Luo X. m(6)A methyltransferase METTL3-mediated lncRNA FOXD2-AS1 promotes the tumorigenesis of cervical cancer. *Mol Therapy Oncolytics*. 2021;22:574–81.
- Liu X, Zhang W, Wan J, Xiao D, Wei M. Landscape and construction of a novel N6-methyladenosine-related lncRNAs in cervical cancer. *Reproductive Sci (Thousand Oaks Calif)*. 2023;30(3):903–13.

23. Chen X, Comish PB, Tang D, Kang R. Characteristics and biomarkers of ferroptosis. *Front Cell Dev Biol.* 2021;9:637162.
24. Tang D, Kroemer G. Ferroptosis. *Curr Biology.* CB. 2020;30(21):R1292–7.
25. Chen X, Kang R, Kroemer G, Tang D. Broadening horizons: the role of ferroptosis in cancer. *Nat Rev Clin Oncol.* 2021;18(5):280–96.
26. Chang X, Miao J. Ferroptosis: mechanism and potential applications in cervical cancer. *Front Mol Biosci.* 2023;10:1164398.
27. Ji X, Qian J, Rahman SMJ, Siska PJ, Zou Y, Harris BK, Hoeksema MD, Trenary IA, Heidi C, Eisenberg R, et al. xCT (SLC7A11)-mediated metabolic reprogramming promotes non-small cell lung cancer progression. *Oncogene.* 2018;37(36):5007–19.
28. Xu Y, Lv D, Yan C, Su H, Zhang X, Shi Y, Ying K. METTL3 promotes lung adenocarcinoma tumor growth and inhibits ferroptosis by stabilizing SLC7A11 m(6)A modification. *Cancer Cell Int.* 2022;22(1):11.
29. Li L, Zeng J, He S, Yang Y, Wang C. METTL14 decreases FTH1 mRNA stability via m6A methylation to promote sorafenib-induced ferroptosis of cervical cancer. *Cancer Biol Ther.* 2024;25(1):2349429.
30. Zhou N, Yuan X, Du Q, Zhang Z, Shi X, Bao J, Ning Y, Peng L. FerrDb V2: update of the manually curated database of ferroptosis regulators and ferroptosis-disease associations. *Nucleic Acids Res.* 2023;51(D1):D571–82.
31. Zhang Y, Guo L, Dai Q, Shang B, Xiao T, Di X, Zhang K, Feng L, Shou J, Wang Y. A signature for pan-cancer prognosis based on neutrophil extracellular traps. *J Immunother Cancer.* 2022;10(6).
32. Ritchie ME, Phipson B, Wu D, Hu Y, Law CW, Shi W, Smyth GK. Limma powers differential expression analyses for RNA-sequencing and microarray studies. *Nucleic Acids Res.* 2015;43(7):e47.
33. Wang W, Lu Z, Wang M, Liu Z, Wu B, Yang C, Huan H, Gong P. The cuproptosis-related signature associated with the tumor environment and prognosis of patients with glioma. *Front Immunol.* 2022;13:998236.
34. Zhao P, Zhen H, Zhao H, Huang Y, Cao B. Identification of hub genes and potential molecular mechanisms related to radiotherapy sensitivity in rectal cancer based on multiple datasets. *J Translational Med.* 2023;21(1):176.
35. Newman AM, Liu CL, Green MR, Gentles AJ, Feng W, Xu Y, Hoang CD, Diehn M, Alizadeh AA. Robust enumeration of cell subsets from tissue expression profiles. *Nat Methods.* 2015;12(5):453–7.
36. Aran D, Hu Z, Butte AJ. xCell: digitally portraying the tissue cellular heterogeneity landscape. *Genome Biol.* 2017;18(1):220.
37. Cui H, Ren X, Dai L, Chang L, Liu D, Zhai Z, Kang H, Ma X. Comprehensive analysis of nicotinamide metabolism-related signature for predicting prognosis and immunotherapy response in breast cancer. *Front Immunol.* 2023;14:1145552.
38. Liberzon A, Subramanian A, Pinchback R, Thorvaldsdóttir H, Tamayo P, Mesirov JP. Molecular signatures database (MSigDB) 3.0. *Bioinf (Oxford England).* 2011;27(12):1739–40.
39. Subramanian A, Tamayo P, Mootha VK, Mukherjee S, Ebert BL, Gillette MA, Paulovich A, Pomeroy SL, Golub TR, Lander ES, et al. Gene set enrichment analysis: a knowledge-based approach for interpreting genome-wide expression profiles. *Proc Natl Acad Sci USA.* 2005;102(43):15545–50.
40. Yu G, Wang LG, Han Y, He QY. ClusterProfiler: an R package for comparing biological themes among gene clusters. *OMICS.* 2012;16(5):284–7.
41. Shangguan W, Hu J, Xie Y, Chen Z, Zhong Q, Zheng Z, Zhu D, Zhang Y, Yang J, Han J, et al. Conditional survival of trimodal therapy for nonmetastatic muscle-invasive bladder cancer: A SEER database analysis. *Cancer Med.* 2022;11(12):2356–65.
42. Yang L, Qu Q, Hao Z, Sha K, Li Z, Li S. Powerful identification of large quantitative trait loci using Genome-Wide R/glmnet-Based regression. *J Heredity.* 2022;113(4):472–8.
43. Ye J, Chen X, Lu W. Identification and experimental validation of Immune-Associate LncRNAs for predicting prognosis in cervical cancer. *OncoTargets Therapy.* 2021;14:4721–34.
44. Craven KE, Gökmen-Polar Y, Badve SS. CIBERSORT analysis of TCGA and METABRIC identifies subgroups with better outcomes in triple negative breast cancer. *Sci Rep.* 2021;11(1):4691.
45. Li T, Fan J, Wang B, Traugh N, Chen Q, Liu JS, Li B, Liu XS. TIMER: A web server for comprehensive analysis of Tumor-Infiltrating immune cells. *Cancer Res.* 2017;77(21):e108–10.
46. Ubago-Guisado E, Rodríguez-Barranco M, Ching-López A, Petrova D, Molina-Montes E, Amiano P, Barricarte-Gurrea A, Chirlaque MD, Agudo A, Sánchez MJ. Evidence update on the relationship between diet and the most common cancers from the European prospective investigation into cancer and nutrition (EPIC) study: a systematic review. *Nutrients.* 2021;13(10).
47. Zhu K, Xiaoqiang L, Deng W, Wang G, Fu B. Development and validation of a novel lipid metabolism-related gene prognostic signature and candidate drugs for patients with bladder cancer. *Lipids Health Dis.* 2021;20(1):146.
48. Zeng D, Ye Z, Shen R, Yu G, Wu J, Xiong Y, Zhou R, Qiu W, Huang N, Sun L, et al. IOBR: Multi-Omics Immuno-Oncology biological research to Decode tumor microenvironment and signatures. *Front Immunol.* 2021;12:687975.
49. Yang W, Soares J, Greninger P, Edelman EJ, Lightfoot H, Forbes S, Bindal N, Beare D, Smith JA, Thompson IR, et al. Genomics of drug sensitivity in cancer (GDSC): a resource for therapeutic biomarker discovery in cancer cells. *Nucleic Acids Res.* 2013;41(Database issue):D955–961.
50. Ruan XF, Wen DT, Xu Z, Du TT, Fan ZF, Zhu FF, Xiao J. Identification and validation of ferroptosis-related prognostic gene signature in patients with cervical cancer. *Translational cancer Res.* 2024;13(7):3382–96.
51. Luo A, Lan X, Qiu Q, Zhou Q, Li J, Wu M, Liu P, Zhang H, Lu B, Lu Y, et al. LncRNA SFTA1P promotes cervical cancer progression by interaction with PTBP1 to facilitate TPM4 mRNA degradation. *Cell Death Dis.* 2022;13(11):936.
52. Huang X, Liu X, Du B, Liu X, Xue M, Yan Q, Wang X, Wang Q. LncRNA LINC01305 promotes cervical cancer progression through KHSRP and exosome-mediated transfer. *Aging.* 2021;13(15):19230–42.
53. Wang C, Zeng J, Li LJ, Xue M, He SL. Cdc25A inhibits autophagy-mediated ferroptosis by upregulating ErbB2 through PKM2 dephosphorylation in cervical cancer cells. *Cell Death Dis.* 2021;12(11):1055.
54. Gu Y, Wu X, Zhang J, Fang Y, Pan Y, Shu Y, Ma P. The evolving landscape of N(6)-methyladenosine modification in the tumor microenvironment. *Mol Ther.* 2021;29(5):1703–15.
55. Elhamamsy AR, Metge BJ, Alsheikh HA, Shevde LA, Samant RS. Ribosome biogenesis: A central player in cancer metastasis and therapeutic resistance. *Cancer Res.* 2022;82(13):2344–53.
56. Zhang Y, Sun D, Song J, Yang N, Zhang Y. Integrated profiles analysis identified a Coding-Non-Coding signature for predicting lymph node metastasis and prognosis in cervical cancer. *Front Cell Dev Biol.* 2020;8:631491.
57. Jia H, Cao M, Hao S, Wang J, Wang J. Prediction of prognosis, immune infiltration and immunotherapy response with N6-methyladenosine-related LncRNA clustering patterns in cervical cancer. *Sci Rep.* 2022;12(1):17256.
58. Yu L, Gao Z, Li Z, Liu P, Gao Y, Liang G. Identification of ferroptosis-related molecular subtypes and a methylation-related ferroptosis gene prognostic signature in cervical squamous cell carcinoma. *J Cancer Res Clin Oncol.* 2023;149(16):14673–89.
59. Wu Q, Ma J, Wei J, Meng W, Wang Y, Shi M. FOXD1-AS1 regulates FOXD1 translation and promotes gastric cancer progression and chemoresistance by activating the PI3K/AKT/mTOR pathway. *Mol Oncol.* 2021;15(1):299–316.
60. Qu W, Wei X, Zhang H, Hou J. FOXD1-AS1 promotes malignant behaviours of prostate cancer cells via the miR-3167/YWHAZ axis. *Andrologia.* 2022;54(1):e14263.
61. Ma Y, Han J, Luo X. FOXD1-AS1 upregulates FOXD1 to promote oral squamous cell carcinoma progression. *Oral Dis.* 2023;29(2):604–14.
62. Quail DF, Joyce JA. Microenvironmental regulation of tumor progression and metastasis. *Nat Med.* 2013;19(11):1423–37.
63. Roma-Rodrigues C, Mendes R, Baptista PV, Fernandes AR. Targeting tumor microenvironment for cancer therapy. *Int J Mol Sci.* 2019;20(4).
64. Yao Y, Yan Z, Li C, Zhang S, Liu S, Zhang X, Shi L, Liu W, Shi L, Yao Y. Association of HLA class I and II genes with cervical cancer susceptibility in a Han Chinese population. *Hla.* 2024;103(1):e15340.
65. Schaafsma E, Fugle CM, Wang X, Cheng C. Pan-cancer association of HLA gene expression with cancer prognosis and immunotherapy efficacy. *Br J Cancer.* 2021;125(3):422–32.

Publisher's note

Springer Nature remains neutral with regard to jurisdictional claims in published maps and institutional affiliations.